Chalcogenide Letters Vol. 20, No. 9, September 2023, p. 663 - 675

Films of copper sulphide doped with nickel for optoelectronics: structural, optical, and magnetic characteristics

M. Ahmed[a], A. Alshahrie[a,b] E. R. Shaaban[c,*]
[a]*Department of Physics: Faculty of Science, King Abdulaziz University, 80203, Jeddah, 21589, Saudi Arabia*
[b]*Center of Nanotechnology, King Abdulaziz University, Jeddah 21589, Saudi Arabia*
[c]*Physics Department, Faculty of Science, Al-Azhar University, Assiut P.O. Box 71452, Egypt*

Copper sulfide nanoparticles have a wide range of applications in various fields, and improving their physical properties is highly desirable. In this study, we investigate the influence of nickel concentrations on the structural, optical, and magnetic characteristics of CuS nanoparticles. The structural properties of $Cu_{1-x}Ni_xS$ (x = 0.00, 0.02, 0.04, 0.06, 0.08, and 0.10) were demonstrated using X-ray diffraction (XRD), which confirmed that all samples have a single hexagonal phase. The Energy Dispersive X-ray Technique (EDAX) was used to investigate the elemental analysis of $Cu_{1-x}Ni_xS$. The XPS study revealed the valence states of Cu, Ni, and S in the $Cu_{0.94}Ni_{0.06}S$ nanoparticles, as well as surface oxidation. The optical characteristics were calculated based on the absorbance optical spectra of the films using a UV-vis-NIR double-beam spectrophotometer in the wavelength range of 400–1000 nm. The optical band gap for CuS and Ni-doped CuS samples decreases as the Ni concentration rises. Magnetic studies (using the M-H curve) demonstrate that 2% and 4% Ni-doped CuS nanoparticles exhibit strong ferromagnetism at ambient temperature and transition to a paramagnetic nature. These results suggest the potential of creating spintronic devices using Ni-doped CuS nanoparticles.

(Received July 20, 2023; Accepted September 20, 2023)

Keywords: CuS:Ni nanoparticles, Morphological and structural analysis, Optical parameters, Magnetic properties

1. Introduction

Semiconductor nanostructures have attracted considerable interest due to their unique properties that cannot be achieved from typical bulk materials. Due to their particular size-dependent features, quantum confinement, and the high surface-to-volume ratio of atoms, they exhibit innovative structural, optical, electrical, and magnetic features [1]. Transition metal chalcogenide compounds are receiving increased interest for their synthesis and characterization at the nanoscale [2].

Covellite copper sulfide (CuS) is an adaptable, accessible, and low-toxicity chalcogenide that has gained attention for its potential uses in a variety of industries, from energy to biomedical [3,4]. CuS is a p-type semiconductor because copper vacancies in the material serve as electron acceptors [5]. It can also be converted into a superconductor at a temperature of approximately 1.6 K [6]. The CuS has some particularities, such as a band gap energy of 2.36 eV, high conductivity, and a good optical absorption coefficient [7]. It has prospective uses in photocatalysis [8], sensors [9], optoelectronic devices [10], photovoltaic cells [11], battery electrodes [12], and tissue imaging [13]. Over the years, CuS nanostructures with different morphologies, such as nanowires [14] nanoparticles [15], nanoplates [16], nanorods [17], nanotubes [18], and nanoribbons [19], have been created using a variety of techniques, including the chemical co-precipitation method [15],

* Corresponding authors: esam_ramadan2008@yahoo.com
https://doi.org/10.15251/CL.2023.209.663

the solvothermal method [20], the combustion method [21], the hydrothermal method [22], and the solid-state reaction method [23].

To manufacture nanostructures with superior optical and electrical properties, several efforts have been undertaken, including the incorporation of transition metal ions into binary semiconductors. Nickel (Ni) is one of the most reactive transition elements and has been added to semiconductors to improve luminescence efficiency [24]. The creation of nanoparticles that possess the correct band gap and exhibit strong room-temperature ferromagnetism with Ni doping suggests that Ni-doped CuS diluted magnetic semiconductor nanoparticles may also be utilized in the development of spintronic devices [25]. Diluted magnetic semiconductors have been the focus of significant research over the past 10 years [26-30], given their realistic magnetic properties and capacity to receive both charges and spin degrees in a single compound. These materials also show potential for the manufacturing of spintronic devices, including spin LEDs, MRAM, spin FETs, and RTDs. In this manuscript, we will synthesize high-quality $Cu_{1-x}Ni_xS$ nanoparticles at different Ni percentages (x = 0.00, 0.02, 0.04, 0.06, 0.08, and 0.10) to investigate the impact of Ni doping on the structural parameters, morphology, optical properties and magnetic properties for spintronics and optoelectronic applications.

2. Experimental studies

Nanocrystalline copper sulfide was synthesized by chemical route. CuS nanocrystalline powder and Ni-doped CuS nanocrystalline powder were prepared as follows:

2.1. Preparing CuS and Ni-doped CuS nanoparticles

A mixture of 2.5 mmol $NiCl_2 \cdot 6H_2O$, and $Cu(NO_3)_2 \cdot 3H_2O$, and 5 mmol sulfur powder with 0.075 g polyvinyl pyrrolidone (PVP) was added to 10 ml ethylene glycol (EG), the mixture was vigorously stirred and then put in an autoclave. The autoclave was sealed and maintained at 150 ^oC for 20 h. The Ni concentration was varied (0.00, 0.02, 0.04, 0.06, 0.08, and 0.10%) by changing the amount of $NiCl_2 \cdot 6H_2O$. After cooling the solution to room temperature, the mixture was centrifuged to produce a black powder of CuS: Ni nanocrystals. At low reaction temperatures, the sulfur reacts with ethylene glycol to form S^{2-} ions slowly, which gives the Ni^{2+} ions enough time to substitute for Cu^{2+} ions to form Ni-doped CuS. Finally, the powder was washed with distilled water and absolute ethanol several times and centrifuged at 3500 rpm. Finally, the products were dried at 70 °C overnight (see Fig. 1).

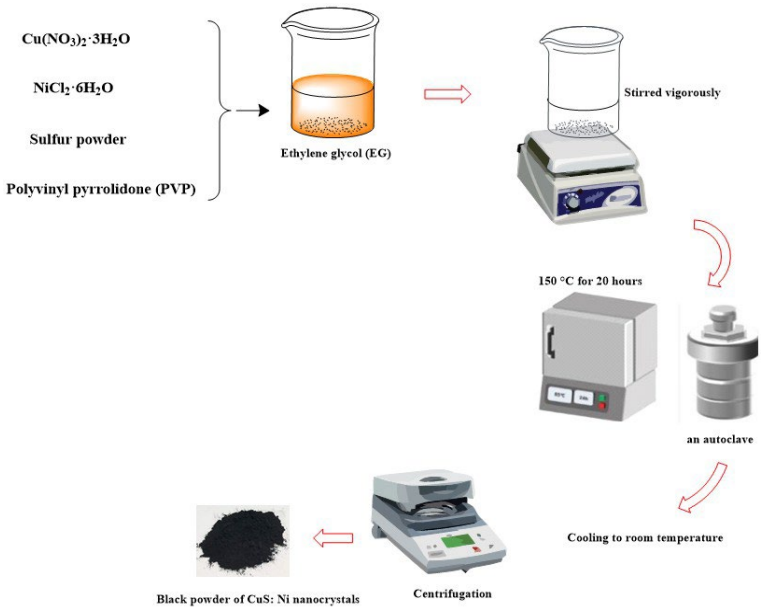

Fig. 1. A diagram explaining the deposition of CuS:Ni nanoparticles.

2.2. Experimental analysis

The structures of pure CuS and Ni-doped CuS samples were investigated using a Philips X-ray diffractometer in the X-mode with Cu-Kα1 radiation. Crystalline silica (99.99%) was used as the interior standard. The elemental composition was measured using energy-dispersive X-ray analysis (EDAX). The surface structure and size were evaluated using transmission electron microscopy (TEM). The characteristics of the band structure were investigated using an XPS technique. The optical absorbance spectra were measured using a UV-vis-NIR double-beam spectrophotometer with a wavelength range of 400–1000 nm. To measure the spectra, 0.01 g of each generated powder was dissolved in a quartz cell with a pure ethanol blank at 25 ^{o}C. We investigated the magnetism of $Cu_{1-x}Ni_xS$ (x = 0.00, 0.02, 0.04, 0.06, 0.08, and 0.10) utilizing field-dependent magnetization (M-H) experiments in magnetic fields up to 40 KG at ambient temperature using a vibrating sample magnetometer model (VSM-9600M-1, USA).

3. Results and discussions

3.1. Structural and Compositional analysis

The XRD patterns of $Cu_{1-x}Ni_xS$ nanoparticles (x = 0.00, 0.02, 0.04, 0.06, 0.08, and 0.10) are demonstrated in Fig. 2. The XRD analysis confirmed that all samples were a single phase of $Cu_{1-x}Ni_xS$ without any additional phases. Moreover, the phase was found to be hexagonal based on JCPDS number 06-0464. Rietveld refinement is a well-established technique for characterizing crystalline materials, as demonstrated in previous studies [31]. The approach involves fitting a theoretical line profile to the measured profile using a least-squares method. Figure 3 displays this method through an example of Rietveld refinement for pure CuS and $Cu_{0.90}Ni_{0.10}S$ nanomaterials. The XRD peaks at 2θ=10.81^{o}, 27.68^{o}, 29.28^{o}, 32.85^{o}, 38.84^{o}, 47.94^{o}, and 59.35^{o} corresponded to the (002), (101), (102), (103), (006), (105), (110), (108), and (116) planes of the $Cu_{1-x}Ni_xS$ hexagonal structure, respectively.

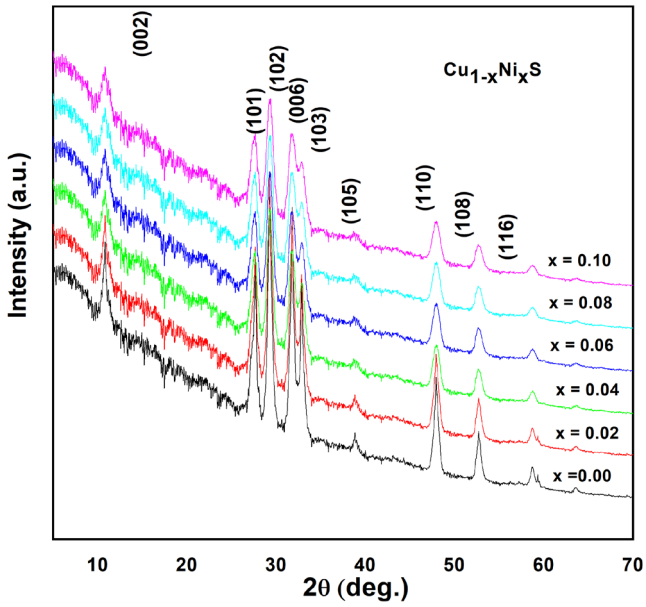

Fig. 2. XRD patterns of $Cu_{1-x}Ni_xS$ nanoparticles.

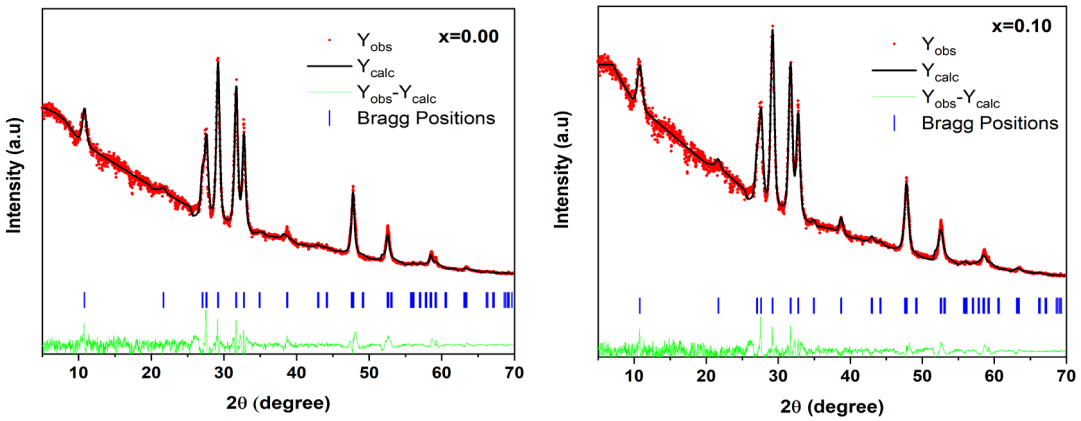

Fig. 3. Rietveld refinement of CuS:Ni nanoparticle for (a) x=0.00 and (b) x=0.10 Ni concentrations.

Due to the large dispersion and low concentration of Ni dopant, no diffraction peaks associated with the expected hybrid phases matching the Ni content were observed within the X-ray resolution limit. It is noteworthy that as the Ni dopant concentration increased, the typical XRD peaks showed minor upward displacement (2θ), which may be due to the similarity between the ionic radius of Ni^{2+} (0.064 nm) and that of its host ion, Cu^{2+} (0.065 nm). Moreover, as the concentration of Ni dopant increased, the intensity of the most notable peaks (103) and (110) gradually reduced, while the FWHM increased, indicating a decrease in the crystalline nature of the samples. Therefore, these results suggest that Ni^{2+} ions integrated at the Cu^{2+} site as substitutional impurities without changing the structure of the $Cu_{1-x}Ni_xS$ phase. Table 1 presents the determined structural parameters such as crystallite size (D), lattice strain (ε), the number of crystallites per unit volume (N_c), and dislocation density (δ), which were calculated using the equations mentioned below [27,29]:

$$D_{(102)} = \frac{0.89\lambda}{\beta \cos\theta} \tag{1}$$

$$\varepsilon = \frac{\beta \cos\theta}{4} \tag{2}$$

$$\delta = \frac{1}{D^2} \tag{3}$$

$$N_c = \frac{d}{D^3} \tag{4}$$

where λ, θ, and β are the wavelength, Bragg's angle (in radians), and the full width at half maximum (FWHM), respectively. After subtracting the instrumental broadening input from the peaks [32,33], the Debye-Scherer formula showed that the estimated crystallization size of the synthesized materials ranged from 7 to 12.7 nm as illustrated in Fig. 4.

Table 1. Structural parameters of Cu_3N thin film.

Ni concentrations (at %)	***Lattice Constant (Å)***		***D (nm)***	***FWHM (2θ)***	***δ ($\times 10^{-3}$) nm^{-2}***	***ε***
	a	***c***				
0.00	*3.807*	*16.40*	*12.7*	*0.34*	*2.2*	*0.0041*
0.02	*3.804*	*16.39*	*12.4*	*0.35*	*3.0*	*0.0060*
0.04	*3.801*	*16.39*	*11.3*	*0.36*	*3.5*	*0.0076*
0.06	*3.799*	*16.38*	*10.0*	*0.39*	*3.8*	*0.0089*
0.08	*3.798*	*16.37*	*8.6*	*0.41*	*4.0*	*0.0096*
0.10	*3.795*	*16.36*	*7.0*	*0.42*	*6.1*	*0.0301*

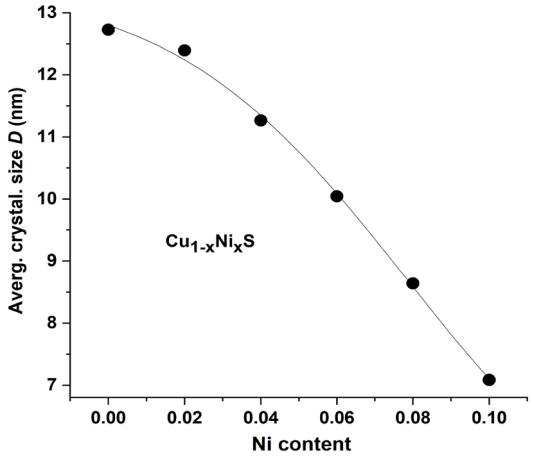

Fig. 4. Average crystallites size versus Ni concentrations of $Cu_{1-x}Ni_xS$ nanoparticles.

The EDAX analysis was performed to provide additional confirmation of the presence of Ni. Fig. 5 displays the EDAX spectra of pure CuS and $Cu_{0.90}Ni_{0.10}S$ nanoparticles, indicating that Ni has been absorbed into the samples as each sample contains either Cu, S, or Ni. The EDAX analysis revealed that the nanoparticles with the selected ratios were almost stoichiometric.

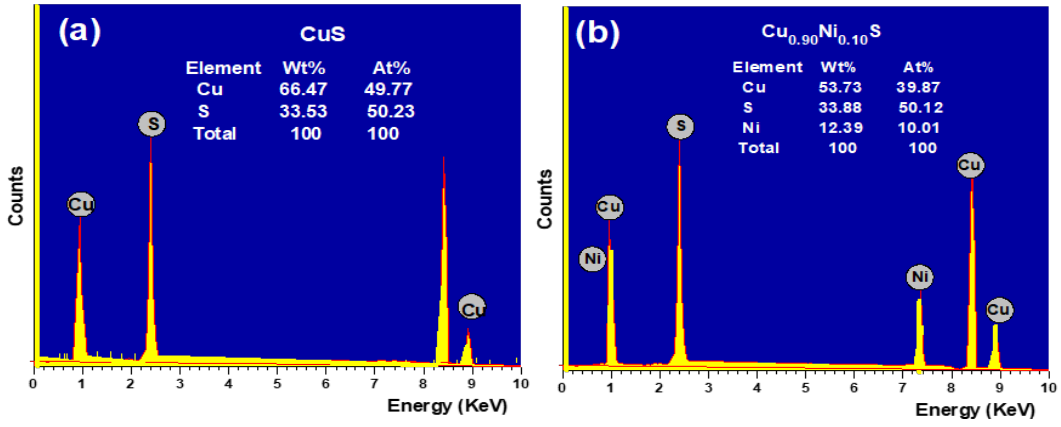

Fig. 5. EDAX spectra of (a) pure CuS and (b) $Cu_{0.90}N_{0.10}S$ nanoparticles.

The surface structure and size were evaluated using transmission electron microscopy (TEM) analysis of prepared samples. Fig. 6 shows the TEM images of samples of pure CuS, $Cu_{0.94}Ni_{0.06}S$, and $Cu_{0.90}Ni_{0.10}S$ nanoparticles. The size of the synthesized samples was determined to be between 7 and 13 nm using TEM analysis, which is in excellent agreement with the crystalline size calculated through XRD analysis.

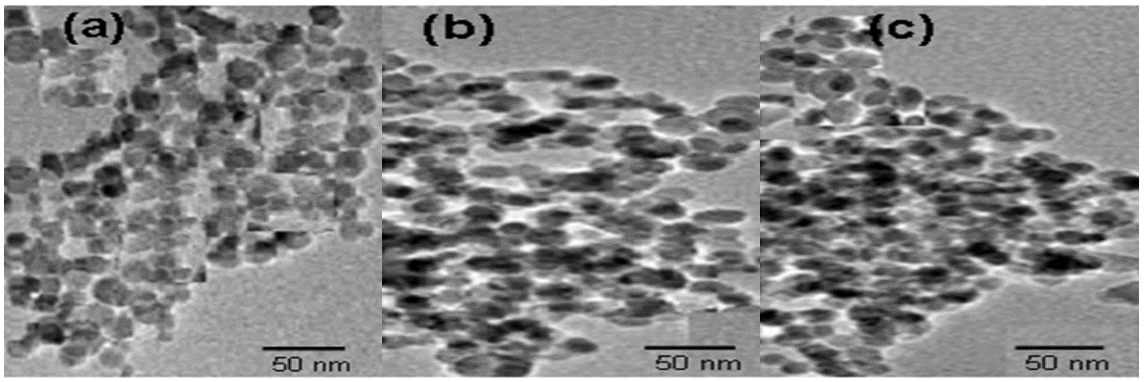

Fig. 6. TEM of (a) pure CuS (b) $Cu_{0.94}N_{0.06}S$ and (c) $Cu_{0.90}N_{0.10}S$ nanoparticles.

Furthermore, an XPS study was conducted to examine the valence state of the components in the $Cu_{0.94}Ni_{0.06}S$ sample. Fig. 7 displays the high-resolution spectra of Cu2p, Ni2p, and S2p elements as well as the assessment spectra of $Cu_{0.94}Ni_{0.06}S$ nanoparticles. The survey spectra of $Cu_{0.94}Ni_{0.06}S$ show signals from Cu, Ni, S, O, and C, with the O1s signal caused by oxygen on the sample surface in the surrounding air (Fig. 7(a)). The high-resolution Cu2p spectrum, shown in Fig. 7(b), presents two peaks at binding energies of 931.9 eV for $Cu2p_{3/2}$ and 951.8 eV for $Cu2p_{1/2}$. There is no peak present in the Cu2p spectrum, indicating the presence of the Cu^{1+} state in the $Cu_{0.94}Ni_{0.06}S$ nanoparticles [34,35]. The Ni 2p spectrum in Fig. 7(c) shows peaks at 852.6 eV for $Ni2p_{3/2}$, 869.7 eV for $Ni2p_{1/2}$, and peaks at 857.7 and 876.8 eV, all of which correspond to the presence of the Ni^{2+} state in the $Cu_{0.94}Ni_{0.06}S$ nanoparticles. The two major peaks seen in the S2p spectrum of Fig. 7(d) were attributed to the binding energies of $S2p_{3/2}$ and $S2p_{1/2}$, which are linked with the S^{2-} signal. The $SO4^{-2}$ signal from sulfur oxidation can be attributed to a modest satellite peak at 167.6 eV, confirming the existence of surface oxidation [36].

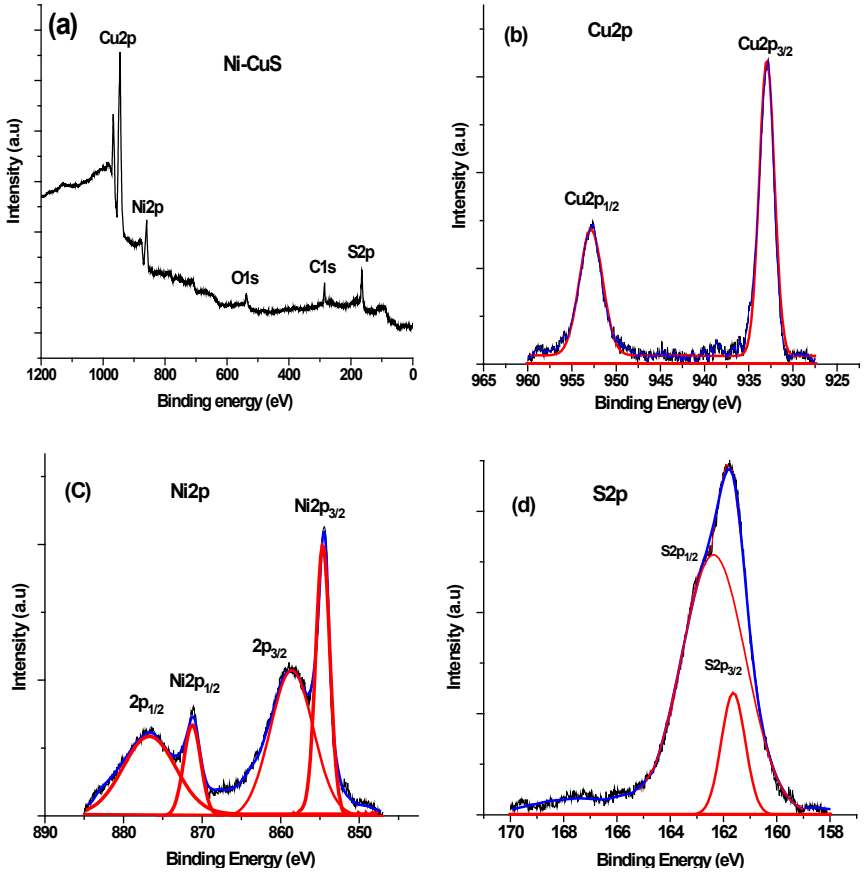

Fig. 7. XPS spectra of (a) $Cu_{0.94}N_{0.06}S$ nanoparticles and (b, c, d) represent the deconvolution of XPS peaks.

3.2. Optical characterization

3.2.1. Absorbance, extension coefficient (k), and absorption coefficient (α)

To better understand the behavior of semiconductor nanostructures, optical absorption measurements are essential. Fig. 8 shows the absorbance spectra of $Cu_{1-x}Ni_xS$ nanoparticles (x = 0.00, 0.02, 0.04, 0.06, 0.08, and 0.10) are shown.

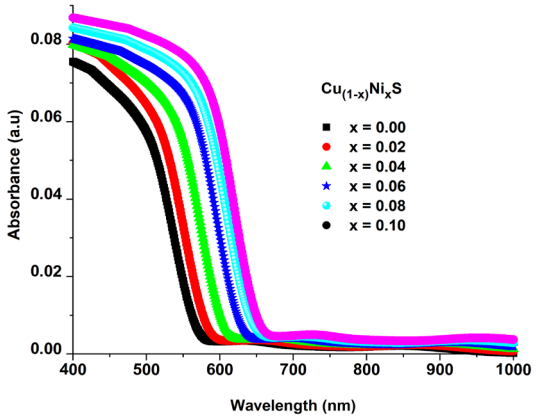

Fig. 8. Absorbance spectra for $Cu_{1-x}Ni_xS$ nanoparticles.

The extinction coefficient (k) is another term for the absorption index (k), which describes how the amplitude of the electric field that was incident is dissipated within the material.

Therefore, it is connected to polarization ability and also provides details on optical loss in a material that is necessary for optoelectronic applications [37]. The extension coefficient (k) values are calculated using the formula [38]:

$$k = \frac{\alpha\lambda}{4\pi} \tag{5}$$

The 'k' values for $Cu_{x-1}Ni_xS$ are presented in Fig. 9.

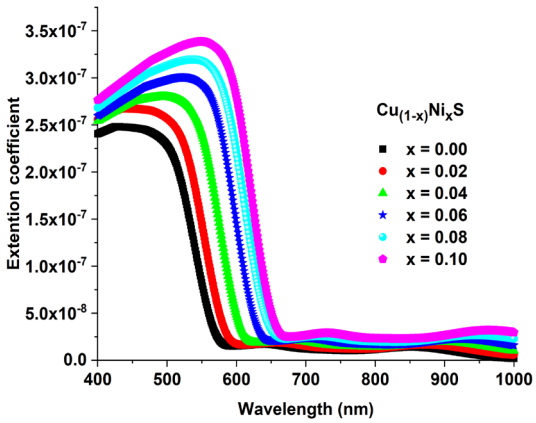

Fig. 9. Extention coefficient for $Cu_{1-x}Ni_xS$ nanoparticles.

The absorption coefficient (α) values are determined from the optical measurements (T and R) and the thickness of the thin layer (*d =1 cm)* as follows [39]:

$$\alpha = \frac{1}{d}\ln\left[\frac{(1-R)^2 + \left[(1-R)^4 + 4R^2T^2\right]^{1/2}}{2T}\right] \tag{6}$$

Figure 10 shows α values at the low wavelength regime that increase with increasing Ni concentrations, indicating the normal dispersion characteristics of the nanoparticles.

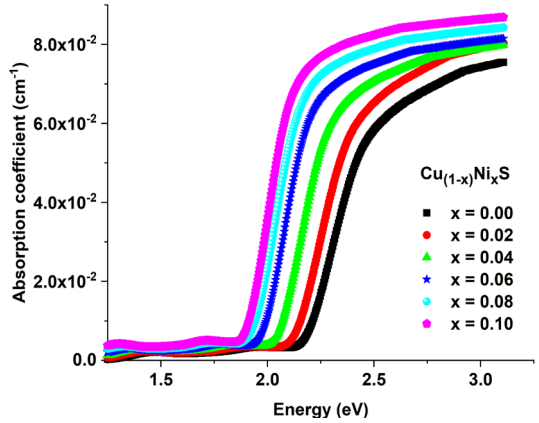

Fig. 10. Absorbance coefficient for $Cu_{1-x}Ni_xS$ nanoparticles.

3.2.2. Optical energy bandgap E_g^{opt}

The optical bandgap E_g^{opt} values for $Cu_{i-x}Ni_x$ (x =0.00, 0.02, 0.04, 0.06, 0.08, and 0.10) are estimated at the high absorption edge using the Tauc equation [40]:

$$\alpha h\nu = A\left(h\nu - E_g^{opt}\right)^p \tag{7}$$

where h is Plank's constant, ν is the frequency of incident radiation, α is the absorption coefficient, and p is considered as 1/2 and 2 for direct and indirect bandgap semiconductors, respectively. Figures 11 and 12 show the values of the direct and indirect energy gaps, respectively. Extrapolating the linear segment of the plot between $h\upsilon$ and $(\alpha h\upsilon)^2$ provides the values of the direct energy gaps (and $(\alpha h\upsilon)^{1/2}$ for indirect) for synthesized nanoparticles. The calculated direct energy gap decreases from 2.26 eV to 1.95 eV with increasing Ni contents in $Cu_{1-x}Ni_xS$, providing direct evidence of quantum confinement associated with the nanoscale regime of the particles. The presence of Ni ions increases the carrier concentration, which leads to the development of defect levels in the optical bandgap and bandgap reduction. Furthermore, the calculated bandgap values from the optical absorption spectra are much closer to those reported in the literature [34,41,42]. Fig. 13 shows the direct and indirect energy gaps as a function of the Ni concentration in the different compositions of $Cu_{1-x}Ni_xS$ nanoparticles.

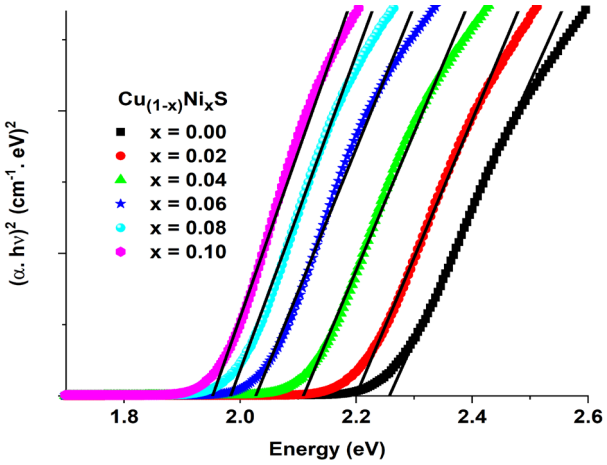

Fig. 11. The calculated values of the direct energy gap for $Cu_{1-x}Ni_xS$ nanoparticles.

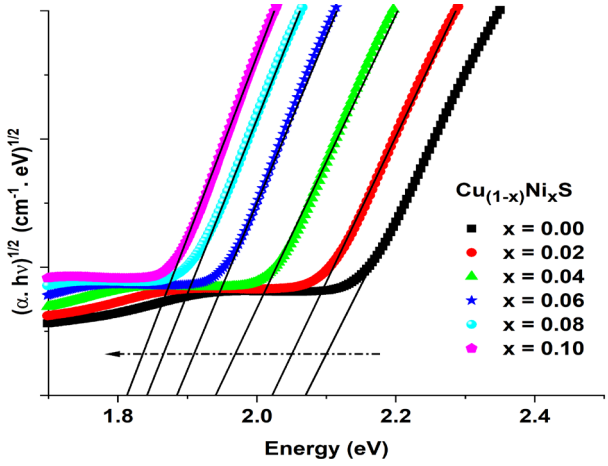

Fig. 12. The calculated values of the indirect energy gap for $Cu_{1-x}Ni_xS$ nanoparticles.

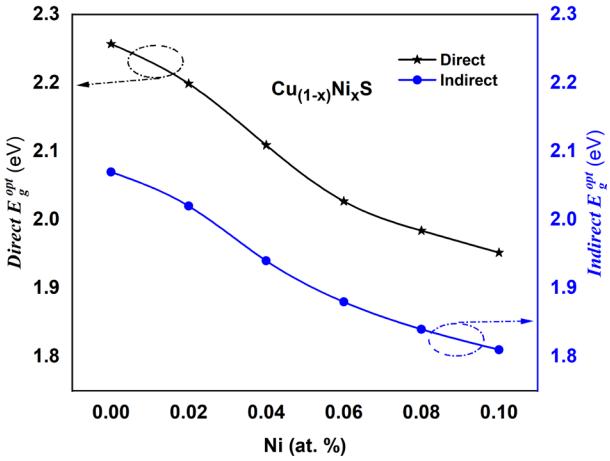

Fig. 13. Direct and indirect energy gap as a function of Ni concentration of the different compositions of $Cu_{1-x}Ni_xS$ nanoparticles.

3.3. Magnetic properties

$Cu_{1-x}Ni_xS$ (x = 0.00, 0.02, 0.04, 0.06, 0.08, and 0.10) nanoparticles were prepared, and magnetic measurements were performed at room temperature using VSM in a range of -15000 G to +15000 G magnetic field to evaluate and realize their magnetic properties (see Fig. 13(a,b). Fig. 13(a) illustrates the effect of Ni^{2+} doping concentration on the magnetization of CuS nanoparticles and indicates that pure CuS samples are diamagnetic due to the absence of lone electrons in the host lattice's "d" orbital. Hysteresis loops are visible in low field areas, suggesting a ferromagnetic nature, and hysteresis loops seem linear with a definite slope in high field areas, showing paramagnetic nature, in the host lattice when Ni dopant concentrations of up to ($x \geq 0.06$) are present.

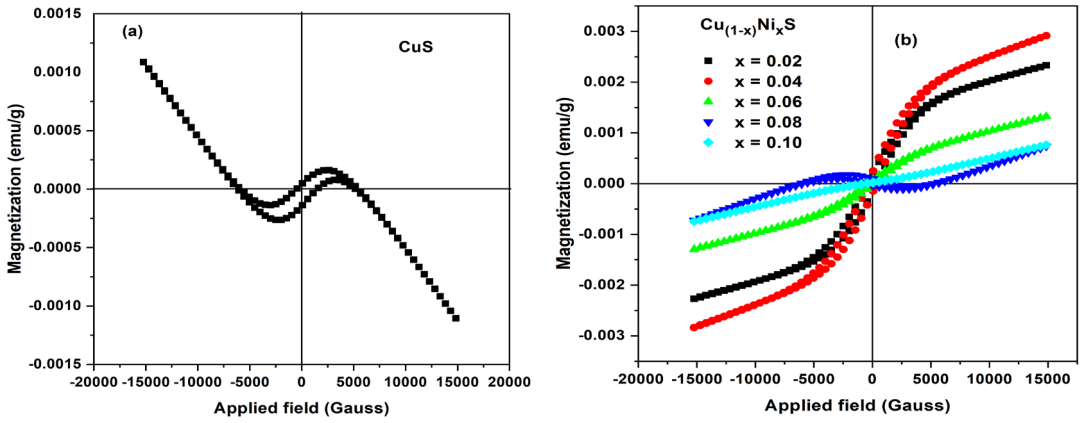

Fig. 14. M-H plots for (a) pure CuS and (b) $Cu_{1-x}Ni_xS$ (x = 0.02, 0.04, 0.06, 0.08, and 0.10) nanoparticles.

The XRD and XPS results reported above provide support for the claim that the generated nanoparticles exhibited no evidence of the parasitic phases linked to the Ni hybrid. These findings demonstrated that the secondary phases were not responsible for the ferromagnetism observed at lower dopant concentrations and lower applied magnetic fields. Many mechanisms, such as the Ruderman Kittel Kasuya Yosida (RKKY) interaction, the bound magnetic polarons (BMPs) notion, the free carrier-mediated exchange, etc., have been proposed to explain the origins of ferromagnetism at ambient temperature. The precise mechanism of intrinsic ferromagnetism in semiconductors doped with transition metal ions but with low magnetic saturation is still being

studied. As seen in Fig. 13**(b)**, $Cu_{1-x}Ni_xS$ (x = 0.02, 0.04) nanoparticles exceed Ni-doped CuS samples in terms of ferromagnetism. This might be a result of double exchange interactions that generate very strong coupling between the spins of neighboring ions' electrons. On the other hand, as the Ni dopant concentration rises ($x \geq 0.06$), the Ni atoms move closer together, and superexchange interferences happen between the neighboring Ni atoms, favoring an antiferromagnetic state [15,44-46].

Furthermore, several tiny ferromagnetic particles in nanoscale materials might only have one magnetic domain, as opposed to the several magnetic domains present in bulk ferromagnetic materials. When a single nanoparticle has a single domain, paramagnetism takes place. In this phenomenon, the magnetizations of the particles are randomly distributed, and they are only aligned with an applied magnetic field. The alignment disappears as soon as the applied field is removed. It's also important to remember that ferromagnetic compounds become unstable when the size of the prepared particles exceeds a certain limit because surface energy provides enough energy for domains to spontaneously shift their polarization directions. The prepared samples consequently underwent a transition from a ferromagnetic environment to a paramagnetic one. Interestingly, K. Subramanyam et al. [46] and Z. H. Wang et al. [47] also discovered the paramagnetic behavior in 7% Ni-doped CuS nanostructures. Based on the aforementioned results, we forecast that 2% and 4% Ni-doped CuS-diluted magnetic semiconductor nanoparticles will be the best materials for spintronic applications.

4. Conclusions

In summary, we determined the structural, optical, and magnetic characteristics of $Cu_{1-x}Ni_xS$ nanoparticles (x = 0.0, 0.02, 0.04, 0.08, and 0.10). All nanoparticles at various Ni concentrations displayed wurtzite-type structures in the XRD patterns. The findings demonstrate that increasing Ni concentration causes nanoparticle size to decrease from 12.7 nm (at x = 0) to 7 nm (at x = 0.10). The calculated direct energy gap decreases from 2.26 eV to 1.95 eV with increasing Ni contents in $Cu_{1-x}Ni_xS$, which is clear proof that quantum confinement is connected to the particles' nanoscale domain. Both the refractive index and the electrical susceptibility as well as the optical conductivity were found to increase with increasing Ni concentrations in $Cu_{i-x}Ni_xS$ nanoparticles. By increasing the concentration of Ni dopant in the CuS host matrix, magnetic tests at room temperature demonstrate that 2% and 4% Ni-doped CuS nanoparticles exhibit good ferromagnetism at room temperature and the transition of magnetic signals from ferromagnetic to paramagnetic nature with increasing Ni dopant concentration ($x \geq 0.06$). The 2% and 4% Ni-doped CuS nanoparticle results are highly suggestive for the creation of spintronic devices.

Acknowledgments

This research work was funded by Institutional Fund Projects under grant no. (IFPIP:1981-130-1443). The authors gratefully acknowledge technical and financial support provided by the Ministry of Education and King Abdulaziz, DSR, Jeddah, Saudi Arabia.

References

[1] Suresh Sagadevan, Jiban Podder, Materials Research, 19. 420-425, (2016); https://doi.org/10.1590/1980-5373-MR-2015-0657

[2] Nouha Loudhaief, Mohamed Ben Salem, Mouldi Zouaoui, Engineering Physics, 4. 7-14, (2020); https://doi.org/10.11648/j.ep.20200401.12

[3] Poulomi Roy, Suneel Kumar Srivastava, CrystEngComm, 17. 7801-7815, (2015); https://doi.org/10.1039/C5CE01304F

[4] Dulce K. Becerra-Paniagua, Evelyn B. Díaz-Cruz, Alejandro Baray-Calderón, Ana R. Garcia-

Angelmo, E. Regalado-Pérez, María del Pilar Rodriguez-Torres, Claudia Martínez-Alonso, Journal of Materials Science: Materials in Electronics, 33. 22631-22667, (2022); https://doi.org/10.1007/s10854-022-09024-9

[5] Joyjit Kundu, Debabrata Pradhan, ACS applied materials, 6. 1823-1834, (2014); https://doi.org/10.1021/am404829g

[6] W Liang, M-H Whangbo, Solid state communications, 85. 405-408, (1993); https://doi.org/10.1016/0038-1098(93)90689-K

[7] M. Rouchdi, H. Mamori, E. Salmani, B. Ait Syad, O. Mounkachi, R. Essajai, H. Ez-zahraouy, H. Chakchak, N. Hassanain, A. Benyoussef, A. El Kenz, A. Mzerd, Applied Physics A, 127. 441, (2021); https://doi.org/10.1007/s00339-021-04589-4

[8] Muhammad Tanveer, Chuanbao Cao, Zulfiqar Ali, Imran Aslam, Faryal Idrees, Waheed S Khan, Faheem K But, Muhammad Tahir, Nasir Mahmood, CrystEngComm, 16. 5290-5300, (2014); https://doi.org/10.1039/c4ce00090k

[9] Hyunju Lee, Sang Won Yoon, Eun Joo Kim, Jeunghee Park, Nano Letters, 7. 778-784, (2007); https://doi.org/10.1021/nl0630539

[10] X-L Yu, C-B Cao, H-S Zhu, Q-S Li, C-L Liu, Q-H Gong, Advanced Functional Materials, 17. 1397-1401, (2007); https://doi.org/10.1002/adfm.200600245

[11] Yixin Zhao, Clemens Burda, Energy Environmental Science, 5. 5564-5576, (2012); https://doi.org/10.1039/C1EE02734D

[12] Chen-Ho Lai, Kuo-Wei Huang, Ju-Hsiang Cheng, Chung-Yang Lee, Bing-Joe Hwang, Lih-Juann Chen, Journal of Materials Chemistry, 20. 6638-6645, (2010); https://doi.org/10.1039/c0jm00434k

[13] Geng Ku, Min Zhou, Shaoli Song, Qian Huang, John Hazle, Chun Li, Copper sulfide ACS nano, 6. 7489-7496, (2012); https://doi.org/10.1021/nn302782y

[14] Matthew T Mayer, Zachary I Simpson, Sa Zhou, Dunwei Wang, Chemistry of Materials, 23. 5045-5051, (2011); https://doi.org/10.1021/cm202564e

[15] N Sreelekha, K Subramanyam, D Amaranatha Reddy, G Murali, S Ramu, K Rahul Varma, RP Vijayalakshmi, Applied Surface Science, 378. 330-340, (2016); https://doi.org/10.1016/j.apsusc.2016.04.003

[16] Haibin Wu, Wei Chen, Nanoscale, 3. 5096-5102, (2011); https://doi.org/10.1039/c1nr10829h

[17] Marta Kruszynska, Holger Borchert, Alicja Bachmatiuk, Mark H Rümmeli, Bernd Büchner, Jürgen Parisi, Joanna Kolny-Olesiak, ACS nano, 6. 5889-5896, (2012); https://doi.org/10.1021/nn302448n

[18] Chunyan Wu, Shu-Hong Yu, Shaofeng Chen, Guannan Liu, Bianhua Liu, Journal of Materials Chemistry, 16. 3326-3331, (2006); https://doi.org/10.1039/b606226a

[19] Changhui Tan, Ran Lu, Pengchong Xue, Chunyan Bao, Yingying Zhao, Materials Chemistry and Physics, 112. 500-503, (2008); https://doi.org/10.1016/j.matchemphys.2008.06.015

[20] Xiao-Sai Hu, Yong Shen, Li-Hui Xu, Li-Ming Wang, Ya-Jun Xing, Journal of Alloys Compounds, 674. 289-294, (2016); https://doi.org/10.1016/j.jallcom.2016.03.047

[21] A Daya Mani, Melepurath Deepa, P Ghosal, CH Subrahmanyam, Electrochimica Acta, 139. 365-373, (2014); https://doi.org/10.1016/j.electacta.2014.07.009

[22] Murugan Saranya, Chella Santhosh, Rajendran Ramachandran, Pratap Kollu, Padmanapan Saravanan, Mari Vinoba, Soon Kwan Jeong, Andrews Nirmala Grace, Powder technology, 252. 25-32, (2014); https://doi.org/10.1016/j.powtec.2013.10.031

[23] Wenzhong Wang, Ling Ao, Materials Chemistry Physics, 109. 77-81, (2008); https://doi.org/10.1016/j.matchemphys.2007.10.035

[24] Abdullah F AL Naim, A Solieman, ER Shaaban, Journal of Materials Science: Materials in Electronics, 31. 3613-3621, (2020); https://doi.org/10.1007/s10854-020-02916-8

[25] Zein K. Heiba, Mohamed Bakr Mohamed, Applied Physics A, 124. 1-11, (2018); https://doi.org/10.1007/s00339-018-1864-2

[26] Meshal Alzaid, WS Mohamed, M El-Hagary, ER Shaaban, NMA Hadia, Optical Materials,

118. 111228, (2021); https://doi.org/10.1016/j.optmat.2021.111228

[27] M Emam-Ismail, M El-Hagary, ER Shaaban, S. Althoyaib, compounds, Journal of alloys, 529. 113-121, (2012); https://doi.org/10.1016/j.jallcom.2012.03.027

[28] ER Shaaban, A Almohammedi, Gomaa AM Ali, Kwok Feng Chong, A Adel, A Ashour, Optik, 164. 527-537, (2018); https://doi.org/10.1016/j.ijleo.2018.03.001

[29] M El-Hagary, ER Shaaban, SH Moustafa, GMA Gad, Solid State Sciences, 91. 15-22, (2019); https://doi.org/10.1016/j.solidstatesciences.2019.03.005

[30] M Emam-Ismail, M El-Hagary, ER Shaaban, S Althoyaib, Journal of alloys compounds, 529. 113-121, (2012); https://doi.org/10.1016/j.jallcom.2012.03.027

[31] Juan Rodriguez-Carvajal, FULLPROF: a program for Rietveld refinement and pattern matching analysis, in satellite meeting on powder diffraction of the XV congress of the IUCr. Toulouse, France:[sn].1990.

[32] Pan-Young Kim, Jai-Yeoul Lee, Hee-Young Lee, Se-Jong Lee, Nam-In Cho, Journal of the Korean Physical Society, 53. 207-211, (2008); https://doi.org/10.3938/jkps.53.207

[33] ER Shaaban, Mansour Mohamed, Mohamed N Abd-el Salam, AY Abdel-Latief, MA Abdel-Rahim, Optical Materials, 86. 318-325, (2018); https://doi.org/10.1016/j.optmat.2018.10.027

[34] Chandu VV Gopi, Sangaraju Sambasivam, Rajangam Vinodh, Hee-Je Kim, Ihab M Obaidat, Journal of Materials Science: Materials in Electronics, 31. 975-982, (2020); https://doi.org/10.1007/s10854-019-02608-y

[35] Beilei Yuan, Qiqian Gao, Xueyu Zhang, Lianfeng Duan, Li Chen, Zhu Mao, Xuesong Li, Wei Lü, Electrochimica Acta, 277. 50-58, (2018); https://doi.org/10.1016/j.electacta.2018.04.218

[36] Hongcheng Ruan, Yafeng Li, Heyuan Qiu, Mingdeng Wei, Journal of alloys compounds, 588. 357-360, (2014); https://doi.org/10.1016/j.jallcom.2013.11.070

[37] Yifei Zhang, Jeffrey B Chou, Junying Li, Huashan Li, Qingyang Du, Anupama Yadav, Si Zhou, Mikhail Y Shalaginov, Zhuoran Fang, Huikai Zhong, Nature communications, 10. 1-9, (2019); https://doi.org/10.1038/s41467-019-12196-4

[38] Ahmed Saeed Hassanien, Journal of Alloys and Compounds, 671. 566-578, (2016); https://doi.org/10.1016/j.jallcom.2016.02.126

[39] Essam R Shaaban, Mohamed Yousry Hassaan, MG Moustafa, Ammar Qasem, Gomaa AM Ali, Optik, 186. 275-287, (2019); https://doi.org/10.1016/j.ijleo.2019.04.097

[40] J Tauc, A Menth, States in the gap, Journal of non-crystalline solids, 8. 569-585, (1972); https://doi.org/10.1016/0022-3093(72)90194-9

[41] V Ramasamy, K Praba, G Murugadoss, Superlattices and Microstructures, 51. 699-714, (2012); https://doi.org/10.1016/j.spmi.2012.02.008

[42] Somayeh Azimi, Alireza Nezamzadeh-Ejhieh, Journal of Molecular Catalysis A: Chemical, 408. 152-160, (2015); https://doi.org/10.1016/j.molcata.2015.07.017

[43] Ahmed Saeed Hassanien, Ishu Sharma, Alaa A. Akl, Journal of Non-Crystalline Solids, 531. 119853, (2020); https://doi.org/10.1016/j.jnoncrysol.2019.119853

[44] S-y Koshihara, A Oiwa, a M Hirasawa, S Katsumoto, Y Iye, C Urano, H Takagi, H Munekata, Physical review letters, 78. 4617, (1997); https://doi.org/10.1103/PhysRevLett.78.4617

[45] Sujit Manna, Subodh Kumar De, Journal of magnetism magnetic materials, 322. 2749-2753, (2010); https://doi.org/10.1016/j.jmmm.2010.04.020

[46] K Subramanyam, N Sreelekha, D Amaranatha Reddy, G Murali, K Rahul Varma, RP Vijayalakshmi, Solid State Sciences, 65. 68-78, (2017); https://doi.org/10.1016/j.solidstatesciences.2017.01.008

[47] Zhen-Hua Wang, Dian-Yu Geng, Ya-Jing Zhang, Zhi-Dong Zhang, CMaterials Chemistry Physics, 122. 241-245, (2010); https://doi.org/10.1016/j.matchemphys.2010.02.042